







Multiple Slips Boundary Layer Flow of Chemically MHD Casson Nanofluid via Homotopic Procedure with Heat Source and Radiation Impacts over an Exponentially Inclined Stretched Surface

Pennelli Saila Kumari¹ , Shaik Mohammed Ibrahim^{1*} , Prathi Vijaya Kumar² , Giulio Lorenzini³ 

¹ Department of Mathematics, Koneru Lakshmaiah Education Foundation, Green Fields, Vaddeswaram 522302, India

² Department of Mathematics, GITAM (Deemed to be University), Visakhapatnam 530045, India

³ Department of Industrial Systems and Technologies Engineering, University of Parma, Parma 43124, Italy

Corresponding Author Email: ibrahimsvu@gmail.com

Copyright: ©2025 The authors. This article is published by IIETA and is licensed under the CC BY 4.0 license (<http://creativecommons.org/licenses/by/4.0/>).

<https://doi.org/10.18280/ijht.430305>

ABSTRACT

Received: 5 April 2025

Revised: 20 May 2025

Accepted: 4 June 2025

Available online: 30 June 2025

Keywords:

nanofluid, multi slip effects, thermal condition, MHD, focus contours, thermophoresis, comparison analysis, heat source

Theoretically, this article investigates the two-dimensional, thermal energy and mass transfer non-Newtonian flow (Casson) over a stretched surface, nanofluid with exponential inclination when there is a heat source and thermal radiation present. It is assumed that a particular exponential function governs the variation of the wall temperature, wall concentration, and stretching velocity. In addition we considered the chemical reactions, solutal slip, velocity slip, thermal slip, and blowing/suction factors. The analytical solution is subsequently obtained using the homotopy analysis method with the assistance of the BVPh2.0 package in Mathematica. The outcomes reveal a direct correlation between various parameters and fluid dynamics. Velocity profiles are enhanced by factors such as the velocity ratio, thermal Grashof and solutal Grashof characteristics, while they diminish with the Casson parameter, velocity slip coefficient, and inclination angle characteristics. Temperature profiles, on the other hand, respond positively to the heat generation/absorption, and thermal radiation but inversely to the thermal slip factor, velocity ratio, and Prandtl number. Concentration profiles exhibit contrasting trends, escalating with the magnetic factor, and thermophoresis characteristics, Casson factor, yet declining with the Brownian motion factor, Schmidt number, and concentration slip characteristics. An analysis of the skin friction coefficient highlights the impact of the Casson characteristics and magnetic characteristics parameter, showcasing they influence fluid flow characteristics. Notably, local heat and mass transfer rates are negatively influenced by the Casson factor and the magnetic coefficient. A comprehensive comparison with existing literature underscores the strong agreement and validation of the current research findings. This approach offers considerable benefits in a wide variety of sectors, such as ecology, bioengineering, geophysics, biomedical, and architectural thermal insulation, amongst others.

1. INTRODUCTION

With varying shear, non-Newtonian fluids' viscosity varies rates and pressures because they don't adhere newtons law on viscosity. Numerous sectors can benefit from studying non-Newtonian fluids. It is well-known that fluids whose behaviour is not in accordance with Newton's laws include things like petroleum, nuclear waste disposal fluids, hydrology of groundwater, systems for cooling transpiration, almond juice, natural honey & other lotions and edible oils required for the body. A threshold stress property is displayed by Casson fluid, of non-Newtonian fluids category. Human blood is a complex fluid that can be classed as a Casson fluid since it contains blood cells, has heat transmission capabilities, and contains complex components like fibrinogen, synovial fluid, and rouleaux. Casson first proposed the rheological model, which is another name for the Casson model [1]. Using thermal radiation and chemical processes as variables, Reddy

[2] performed theoretical research on the multi-harmonic flow of connected boundary layers through a porous medium of a Casson fluid over a stretched surface with an exponential inclination. A fluid of Casson model within a tube flow of blood was developed by Walawender et al. [3], and the basic assets of Casson fluid in pipes within a similar kind of absorbent channel were studied by Dash et al. [4]. Researchers Mukhopadhyay et al. [5] looked into the time-dependent flow on a stretchy surface of Casson fluid with double dimension. Casson fluid's boundary layer flow (BL) of thermal energy transfer towards a stretching top surface had been studied by Pramanik [6], who took blowing and suction effects into account. Rao et al. [7] applied similar transformation techniques of triple-dimensional flow of Casson motion upon a stretched membrane with various parameters.

Heat transfer fluids like engine oils, ethylene glycol and water, known for their low thermal conductivity are termed base fluids. The thermal energy exchange capabilities of the

base fluid are substantially enhanced by adding nanoparticles to the base fluid to form nanofluids. Nanoparticles are nano-sized particles (1-100 nm) which when added to the base fluid exhibit improve the nanofluid's thermal energy transfer properties. Choi [8] was the first to investigate thermal behaviour of nanofluids and the study revealed that nanofluids enhance the heat transfer rate. Reddy and Ramasekhar [9] investigated enhancement of heat transfer and operational performance using nanofluid in engine oil. Dzulkifli et al. [10] investigated heat transfer and unsteady flow in a Cu-water nanofluid across a stretching sheet. They discovered that as the unsteadiness parameter and nanoparticle volume fraction increase, the skin friction coefficient decreases.

An integrated fluid system that exhibits properties of nanofluids, magneto-hydrodynamics (MHD), and non-Newtonian fluids (Casson) is called a magneto-Casson nanofluid. Consisting of a base fluid—which may or may not be conducting—with suspended nanoparticles, behaving Casson as a fluid, and being affected by an applied magnetic field. These fluids have potential in cutting-edge heat transfer applications that make use of magnetic fields, such as non-Newtonian fluidic systems for magnetically enhanced heat transfer, magnetic hyperthermia to treat cancer, and magnetic drug targeting.

Electromagnetic waves may travel in any direction and are known as radiation. The radiation that an object emits determines its classification. Ionizing and non-ionizing radiations are the two main categories of radiation. A number of fields rely heavily on radiation, including engineering, astronomy, and climate science. To design solar panels, study the distribution of energy on Earth, and assess heat transmission in industrial processes, one must have a thorough understanding of radiation.

The Casson nanofluid's magnetohydrodynamic (MHD) flow on a surface that is not stationary and is shrinking is examined by Lund et al. [11]. Shah et al. [12] derived the magneto hydrodynamic flow of Casson nanofluid time-fractional method by applying the generalized Fourier and Fick's laws over a slanted channel. The magneto hydro dynamic Couple stress Casson flow of a hybrid nanofluid was explored by Rehman et al. [13]. Due to its significant uses in modern engineering devices, specifically by improving heat management and efficacy in several industrial processes, the stress of the MHD Couple Rehman et al. [13] looked into the Casson flow of a hybrid nanofluid. Panigrahi et al. [14] suggested an analysis to an inclined magnetic field affects Casson nanofluid flowing across an extending spread sheet that's embedded into a porous matrix with saturation. Irshad et al. [15] studied a challenging numerical problem involving the magnetohydrodynamic Casson nanofluid flow in a porous medium across a stretched membrane. They used the Keller box technique, which relies on the finite difference method (FDM), to solve this issue.

The flow of nanofluids towards a heated permeable sheet with extensions and compressions in the MHD stagnation area, where fluid velocity tends to be zero, was investigated by Chaudhary and Kanika [16]. They investigated the heat production and absorption, as well as thermal radiation, influenced the flow of nanofluids. An investigation was conducted by Reddy et al. [17] to determine the impact that thermal radiation has on the magneto hydrodynamic boundary layer flow of a non-Newtonian nanofluid as it travels across a stretched surface that contains porous media.

Nanofluid flow across a stretching sheet in a porous media

was the subject of an investigation by Pal and Mandal [18], who looked into the ways in which thermal radiation and chemical reactions influence mass transfer and mixed convection heat. The thermal and stratification properties of non-Newtonian fluids that are flowing across porous media were explored by Megahed and Abbas [19]. The FDM utilized by Barik et al. [20] in order to explore the effects of repeated slips on the flow of MHD nanofluids across a stretched sheet that was both chemically reactive and radiative. The sheet was also inclined.

The impact of dual stratification on the stagnation point had been investigated by Sadaf et al. [21]. They considered the radiative Riga plate flow of Walters' B nanofluid. Ramana et al. [22] provided an explanation of the continuous magnetohydrodynamic stagnation point fluid flow for a fluid of Casson across a stretched sheet with a source of heat and a first-order reaction of a chemical by including multiple slip boundary conditions. According to their observations, the thermal profile and chemical reactivity decreased when the heat source and chemical reaction parameters rose. In order to study the problem of stagnating location (where fluid velocity tends to zero) flow of MHD methanol-based nanofluid through convectively heated stretched sheets while keeping in mind the influence of heat radio activity and generation via a porous medium, Nandi et al. [23] used statistical and numerical perspectives.

Particles in fluids, particularly those at the microscopic level, are controlled by two separate systems: thermophoretic diffusion and Brownian motion. Particles in a liquid or gas can be described by the random and unexpected motion that occurs when they collide with the molecules of the fluid, a process known as Brownian motion. When there is a change in temperature throughout a fluid, this process is called thermophoretic diffusion. When there is a difference in temperature between the fluid and the particles move from hotter to colder areas by a process called thermophoresis. Particle displacement in fluids is a common feature of both Brownian motion and thermophoretic diffusion, yet these two phenomena have different origins. Thermophoretic diffusion happens when particles interact with the temperature differential in the fluid, as opposed to Brownian motion, which is primarily produced by random collisions with molecules in the fluid. Microfluidic device creation, colloidal system analysis, and atmospheric dynamics understanding are just a few of the scientific and technological fields that rely on these two phenomena.

In order to investigate the effects of Brownian motion, thermophoretic diffusion, and thermal advancement across an incline on MHD micropolar nanofluid, Thabet et al. [24] utilized computer simulations to investigate the interaction between these three phenomena. In their study, Shahzad et al. [25] investigated the Darcy-Forchheimer flow of bioconvective micropolar nanofluid between two discs with Cattaneo-Christov heat flux. They also investigated the relationship between thermophoretic diffusion and Brownian motion. Hazarika and Ahmed [26] conducted research on thermophoresis and Brownian motion in micro-polar nanofluids by employing the bvp4c numerical approach. Irfan [27] conducted a study in which he explored the effects of diffusion through thermophoresis and Brownian motion. The study involved Carreau nanofluids in a non-linear convectational mixed flow of nanofluids with varying parameters. Shah et al. [28] observed diffusion effects of thermophoretics and Brown's law in their research on the

MHD dynamics with Higher-Convection flow of Maxwell nanofluids down a typically inclined surface. This research was conducted in addition to the MHD dynamics. Recently, literature in this field has drawn on thermophoretic transmission and Brownian law studies [29-34].

A fluid's movement across a surface area that is sloping or inclined in relation to a straight line is referred to as fluid movement across a surface with inclination. Gravitational forces, fluid viscosity, and gradient are some of the variables that might affect this flow was studied by Pera and Gebhart [35]. The value-based study of MHD free convective layer of limitations motion of Casson substance brought on by a porous surface that is angled vertically, as well as the consequences of thermal energy and chemical changes, was reported by Raju [36]. Rafique et al. [37] used the Soret and Dufour effect to study the Casson Nanofluid limit layer's movement on a sloped elongated surface area. Tawade et al. [38] used the Runge-Kutta 4th-order with the shooting technique for resolving ordinary differential calculations that are non-linear for nanofluid movement that was smooth and unsteady past stretching surfaces in double dimensions. Additional issues about fluid flow beneath a stretchy sheet with varying thicknesses under various circumstances can be found in the literature by Pal et al. [39] and Abbas and Megahed [40].

Mathematica is a sophisticated numerical tool that is known for its efficiency and accuracy in solving nonlinear boundary value problems. This research makes use of the Homotopy Analysis Method (HAM) technique with the assistance of the BVPh2.0 package in Mathematica with the intention of achieving similar results. An efficient framework for numerical calculations in fluid dynamics is provided by HAM, which is characterized by its compact support and qualities that pertain to multiple solutions. Due to the fact that the HAM method incorporates the benefits of various strategies that are designed to handle complicated systems in an effective manner, it is particularly well-suited for the challenge at hand. The purpose of this study is to evaluate the influence that various parameters, including the intensity of the magnetic field, the features of the Casson fluid, the Prandtl quantity, and the velocity ratio, as well as the impacts of multi slip, have on the distributions of velocity, concentration, and temperature. In addition, important technical metrics like as the Sherwood number, the Nusselt number, and the skin friction coefficient are evaluated using this process. The findings provide important insights into the interaction between magnetic fields, non-Newtonian fluid dynamics, and heat transfer. These discoveries have substantial implications for the optimization of industrial processes and the improvement of engineering systems.

2. RESEARCH QUESTION

(1) How do thermal radiation and heat source influence the boundary layer flow and features of thermal transmission of Casson nanofluids?

(2) What is the impact of Brownian motions and thermophoresis's on the flow, thermal, and concentration profiles of Casson nanofluids in the presence of multiple slip effects?

(3) In what ways can magnetohydrodynamics (MHD) enhance or reduce the efficiency of heat transfer in Casson nanofluids?

(4) How can the HAM technique solver be utilized

effectively to predict the implication of Casson fluid factors on thermal and flow distributions?

(5) What is the role of Schmidt number and Prandtl number in optimizing heat transfer and flow dynamics in a Casson nanofluid system?

3. PHYSICAL AND MATHEMATICAL MODELLING

Take note of a stable, two-dimensional Casson flow of nanofluids over a substantially elongated sheet that is disposed at an inclined angle Ω with its perpendicular axis. The x - and y - As shown, the axes are normal to the surface and aligned along the inclined surface in Figure 1. Here, elongating and liberated fluid Acceleration of streams are represented as and $U_{\infty}(x) = be^{\frac{x}{L}}$ correspond, where a and b are any constants, x is the value of regulated together the surface that is being stretched and L is the sheet length. The temperature near and distant from surface are denoted as T_w and T_{∞} , respectively, whereas concentration C_w and C_{∞} are also respectively. A Horizontal electromagnetic nonuniformity induction of strength $B(x) = B_0 e^{\frac{x}{L}}$ is applied parallel to y axis, where B_0 is the uniform magnetic induction power. It is assumed that the magnetic field generated by the fluctuating electrical current is negligible. Furthermore, it is assumed that there is no external electric field and that the charge polarization-induced electrical field is insignificant. In Figure 1, the flow is described. Brownian motion and thermophoresis properties are considered. Chemical responses, the vacuum, injection, thermal energy, and multi-slip effects are also discussed.

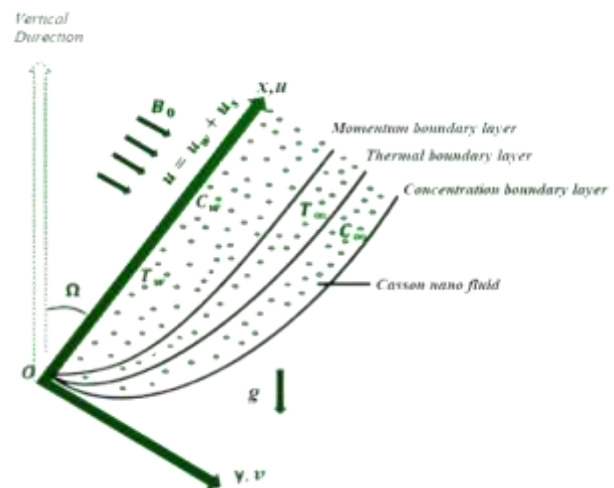


Figure 1. An actual physical manifestation of the flow

The rheological computation of state is presented as follows within the framework of a Casson fluid flow that is isotropic and incompressible:

$$\tau_{ij} = \begin{cases} 2 \left(\mu_B + \frac{p_y}{\sqrt{2\pi}} \right) e_{ij}, & \pi > \pi_c \\ 2 \left(\mu_B + \frac{p_y}{\sqrt{2\pi_c}} \right) e_{ij}, & \pi_c > \pi \end{cases}$$

here, μ_B is the non-Newtonian fluid's material elasticity. p_y is the fluid's stress due to yield, π is the item of the component of

distortion rate in relation to itself, e_{ij} is the (ij) th part of the amount of distortion and π_c is a critical value of this item based on the model that is not Newtonian. Regarding the particular situation of Casson fluid, we considered $\pi > \pi_c$ and $p_y = \frac{\mu_B \sqrt{2\pi}}{\beta}$, it is possible in other words, the fluctuating of the consistency $\mu = \mu_B + \frac{p_y}{\sqrt{2\pi}}$.

Changing the amount of p_y in μ , we get:

$$\mu = \mu_B \left(1 + \frac{1}{\beta} \right)$$

For this investigation, the process of mathematical equations is provided by [41]:

$$\frac{\partial u}{\partial x} + \frac{\partial v}{\partial y} = 0, \quad (1)$$

$$\begin{aligned} u \frac{\partial u}{\partial x} + v \frac{\partial u}{\partial y} &= \nu \left(1 + \frac{1}{\beta} \right) \frac{\partial^2 u}{\partial y^2} \\ &+ g \left[\beta_T (T - T_\infty) + \beta_C (C - C_\infty) \right] \cos \Omega \\ &+ U_\infty \frac{dU_\infty}{dx} + \frac{\sigma_f B^2(x)}{\rho_f} (U_\infty - u), \end{aligned} \quad (2)$$

$$\begin{aligned} u \frac{\partial T}{\partial x} + v \frac{\partial T}{\partial y} &= \alpha \frac{\partial^2 T}{\partial y^2} + \tau \left[D_B \frac{\partial C}{\partial y} \frac{\partial T}{\partial y} + \frac{D_T}{T_\infty} \left(\frac{\partial T}{\partial y} \right)^2 \right] \\ &+ \frac{Q_0}{(\rho c)_f} (T - T_\infty) - \frac{1}{(\rho c)_f} \frac{\partial q_r}{\partial y} \end{aligned} \quad (3)$$

$$u \frac{\partial C}{\partial x} + v \frac{\partial C}{\partial y} = D_B \frac{\partial^2 C}{\partial y^2} + \frac{D_T}{T_\infty} \frac{\partial^2 T}{\partial y^2} - Kr(C - C_\infty) \quad (4)$$

Following Rao [41], the circumstances surrounding limits are considered as:

$$\begin{aligned} u &= U_w(x) + \delta_1^* \left(1 + \frac{1}{\beta} \right) \left(\frac{\partial u}{\partial y} \right), \quad v = V_w, \\ T &= T_w(x) + \delta_2^* \left(\frac{\partial T}{\partial y} \right), \quad C = C_w(x) + \delta_3^* \left(\frac{\partial C}{\partial y} \right) \quad \text{at } y = 0 \\ u &\rightarrow U_\infty, \quad T \rightarrow T_\infty + T_0 e^{x/(2L)}, \\ C &\rightarrow C_\infty + C_0 e^{x/(2L)} \quad \text{as } y \rightarrow \infty, \end{aligned} \quad (5)$$

where,

$$\alpha = \frac{k}{(\rho c)_f}, \quad \nu = \frac{\mu}{\rho_f}, \quad \tau = \frac{(\rho c)_p}{(\rho c)_f}, \quad V_w(x) = V_0 e^{x/(2L)}$$

Following the thermal flux, using the Roseland estimation, is

$$q_r = -\frac{4\sigma^*}{3\kappa^*} \frac{\partial T^4}{\partial y} \quad (6)$$

where, σ^* is Stefan Boltzmann constant and average value of consumption is κ^* . Furthermore, we assume that the internal

flow thermal difference is sufficiently wide, so that T^4 is shown as an inverse function of temperature. Therefore, by enlarging T^4 in Taylor's sequence regarding T_∞ and if we neglect higher order words, we get:

$$T^4 \cong 4T_\infty^3 T - 3T_\infty^4, \quad (7)$$

Making use of Eqs. (6) and (7) the Eq. (3) converts into:

$$\begin{aligned} u \frac{\partial T}{\partial x} + v \frac{\partial T}{\partial y} &= \left(\alpha + \frac{16\sigma^* T_\infty^3}{3\kappa^* (\rho c)_f} \right) \frac{\partial^2 T}{\partial y^2} \\ &+ \tau \left[D_B \frac{\partial C}{\partial y} \frac{\partial T}{\partial y} + \frac{D_T}{T_\infty} \left(\frac{\partial T}{\partial y} \right)^2 \right] + \frac{Q_0}{(\rho c)_f} (T - T_\infty), \end{aligned} \quad (8)$$

The non-linear partial differential equations are reduced to non-linear ordinary differential equations by applying the following similarity transformations.

$$\left. \begin{aligned} \zeta &= \left(\frac{a}{2\nu L} \right)^{1/2} e^{x/(2L)} y, \quad u = a e^{x/L} f'(\zeta), \\ v &= -\sqrt{\frac{\nu a}{2L}} e^{x/(2L)} (f(\zeta) + \zeta f'(\zeta)), \\ T &= T_w = T_\infty + T_0 e^{x/(2L)} \theta(\zeta), \\ C &= C_w = C_\infty + C_0 e^{x/(2L)} \phi(\zeta). \end{aligned} \right\} \quad (9)$$

where, ζ is the similarity variable.

Substituting Eq. (9) in Eqs. (2), (4), and (8), we obtain:

$$\begin{aligned} \left(1 + \frac{1}{\beta} \right) f''' + ff'' - 2f'^2 + 2A^2 + M(A - f') \\ + (Gr\theta + Gc\phi) \cos \Omega = 0, \end{aligned} \quad (10)$$

$$\begin{aligned} \left(1 + \frac{4}{3} R \right) \theta'' + Pr(f\theta' - f'\theta) + Pr Nb \phi' \theta' \\ + Pr Nt \theta'^2 + Pr Q \theta = 0, \end{aligned} \quad (11)$$

$$\phi'' + Sc(f\phi' - f'\phi - \gamma\phi) + \frac{Nt}{Nb} \theta'' = 0. \quad (12)$$

The limited conditions are:

$$\begin{aligned} f(0) &= S, \quad f'(0) = 1 + \delta_1 \left(1 + \frac{1}{\beta} \right) f''(0), \\ \theta(0) &= (1 + \delta_2 \theta'(0)), \quad \phi(0) = (1 + \delta_3 \phi'(0)), \\ f'(\infty) &\rightarrow A, \quad \theta(\infty) \rightarrow 0, \quad \phi(\infty) \rightarrow 0, \end{aligned} \quad (13)$$

where,

$$\begin{aligned} \beta &= \frac{\mu_B \sqrt{2\pi}}{p_y}, \quad M = \frac{2L\sigma_f B_0^2}{\rho_f a}, \quad Gr = \frac{Gr_x}{Re_x^2}, \quad A = \frac{b}{a}, \\ Gr_x &= \frac{2Lg\beta_T (T_w - T_\infty)x^2}{a^2}, \quad Gr = \frac{Gr_x}{Re_x^2}, \quad Sc = \frac{\nu}{D_B}, \end{aligned}$$

$$Gc_x = \frac{g2L\beta_c(C_w - C_\infty)x^2}{a^2}, \quad Gc = \frac{Gc_x}{Re_x^2}, \quad Pr = \frac{\nu}{\alpha},$$

$$Nb = \frac{\tau D_B(C_w - C_\infty)}{\nu}, \quad Nt = \frac{\tau D_T(T_w - T_\infty)}{\nu T_\infty},$$

$$\gamma = \frac{2Lk_0}{U_0}, \quad R = \frac{4\sigma^* T_\infty^3}{k^* k}, \quad \delta_1 = \delta_1^* \sqrt{\frac{a}{2Lv}},$$

$$\delta_2 = \delta_2^* \sqrt{\frac{a}{2\nu L}}, \quad \delta_3 = \delta_3^* \sqrt{\frac{a}{2Lv}}, \quad S = -\frac{V_w}{\sqrt{av}},$$

$$Q = \frac{Q_0}{a(\rho c)_f}, \quad Re_x = \frac{ax e^{x/L}}{\nu}.$$

The primary physical factors that are relevant to this topic right now are $Sh_x \left(= \frac{xq_m}{k(C_w - C_\infty)} \right)$ is the local Sherwood number, $Nu_x \left(= \frac{xq_w}{k_\infty(T_w - T_\infty)} \right)$, is the local Nusselt number, $C_f \left(= \frac{\tau_w}{\rho U_w^2} \right)$, is the local Skin-friction component.

Here, wall-shear stress $\tau_w = \mu_B \left(1 + \frac{1}{\beta} \right) \left(\frac{\partial u}{\partial y} \right)_{y=0}$, wall heat flux $q_w = \left(- \left(k_\infty + \frac{16\sigma^* T_\infty^3}{3k^*} \right) \left(\frac{\partial T}{\partial y} \right)_{y=0} \right)$, mass flux $q_m = - \left(D_B \left(\frac{\partial C}{\partial y} \right)_{y=0} \right)$.

With the modifications described above, we have:

$$Re_x^{-1/2} Sh_x = -\phi'(0),$$

$$Re_x^{-1/2} Nu_x = - \left(1 + \frac{4}{3} R \right) \theta'(0),$$

$$Re_x^{1/2} C_f = \left(\left(1 + \frac{1}{\beta} \right) f''(0) \right).$$

4. HAM

It is demonstrated that the Homotopy Analysis Method (HAM), also known as the Homotopy Analysis Method, is an effective semi-analytical method by the fact that it is utilized in a variety of research projects to handle boundary layer flow issues. As an illustration, it has been successfully utilized to acquire semi-analytical solutions for the thermal convection boundary layer flow of incompressible Casson fluids. These solutions incorporate features such as suction/injection and heat sink effects, both of which are essential in polymer coating applications. In addition, the ability of HAM to handle non-linear boundary value problems has been demonstrated by the fact that it has been utilized to produce mathematical expressions for velocity, heat and mass transfer in boundary layer flows that involve thermal radiation in presence of multiple slip effects. The approach has also been utilized in the field of MHD, which has shed light on the impact that parameters like magnetic and Prandtl numbers have on flow characteristics. Additionally, the BVP4.0 program has the capability to ease the implementation of HAM, which enables the efficient computing of solutions in complicated boundary layer situations that involve nanofluids and Casson fluids.

Employing the HAM allowed us to derive the analytic

solutions for Eqs. (10) to (12) with the prescribed boundary conditions (13), using selected initial guesses and linear operators for the functions f, θ and ϕ .

We consider the initial hypotheses and linear operators in the following manner in order to capture the homotopic solutions of Eqs. (10) to (13). The flow chart is given in Figure 2.

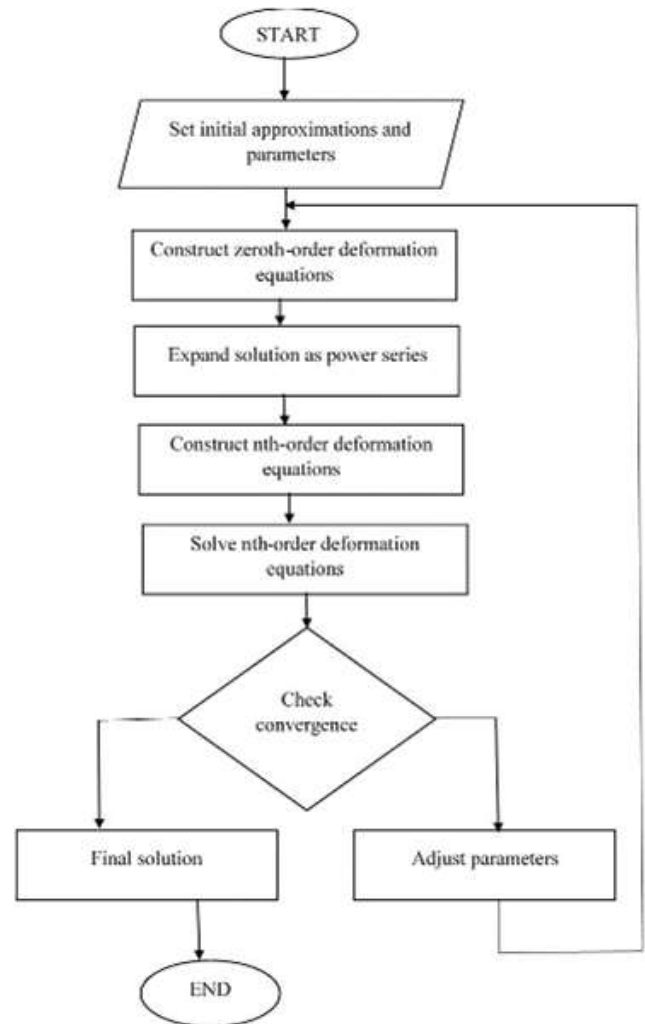


Figure 2. Diagrammatic representation of HAM process

$$f_0(\zeta) = S + A\zeta + \left(\frac{1-A}{1+\delta_1 \left(1 + \frac{1}{\beta} \right)} \right) (1 - e^{-\zeta}),$$

$$\theta_0(\zeta) = \frac{e^{-\zeta}}{1+\delta_2},$$

$$\phi_0(\zeta) = \frac{e^{-\zeta}}{1+\delta_3},$$

$$M_f(f) = f''' - f',$$

$$M_\theta(\theta) = \theta'' - \theta,$$

$$M_\phi(\phi) = \phi'' - \phi,$$

with

$$\begin{aligned}M_f(D_1 + D_2 e^\zeta + D_3 e^{-\zeta}) &= 0, \\M_\theta(D_4 e^\zeta + D_5 e^{-\zeta}) &= 0, \\M_\phi(D_6 e^\zeta + D_7 e^{-\zeta}) &= 0,\end{aligned}$$

where, F_i ($i=1$ to 7) are the arbitrary constants.

The zeroth-order stretching formulas are constructed by us:

$$\begin{aligned}(1-s)M_f(f(\zeta;s)-f_0(\zeta)) \\= p h_f N_f[f(\zeta;s), \theta(\zeta;s), \phi(\zeta;s)],\end{aligned}\quad (14)$$

$$\begin{aligned}(1-s)M_\theta(\theta(\zeta;s)-\theta_0(\zeta)) \\= p h_\theta N_\theta[f(\zeta;s), \theta(\zeta;s), \phi(\zeta;s)],\end{aligned}\quad (15)$$

$$\begin{aligned}(1-s)M_\phi(\phi(\zeta;s)-\phi_0(\zeta)) \\= p h_\phi N_\phi[f(\zeta;s), \theta(\zeta;s), \phi(\zeta;s)],\end{aligned}\quad (16)$$

based on limited circumstances:

$$\begin{aligned}f(0;s) &= S, \\f'(0;s) &= \left[1 + \delta_1 \left(1 + \frac{1}{\beta}\right) f''(0)\right], \\f'(\infty;s) &= 0, \\ \theta(0;s) &= [1 + \delta_2 \theta'(0)], \quad \theta(\infty;s) = 0, \\ \phi(0;s) &= [1 + \delta_3 \phi'(0)], \quad \phi(\infty;s) = 0,\end{aligned}\quad (17)$$

where,

$$\begin{aligned}N_f[f(\zeta;s), \theta(\zeta;s), \phi(\zeta;s)] &= \left(1 + \frac{1}{\beta}\right) \frac{\partial^3 f(\zeta;s)}{\partial \zeta^3} \\&+ f(\zeta;p) \frac{\partial^2 f(\zeta;s)}{\partial \zeta^2} - 2 \left(\frac{\partial f(\zeta;s)}{\partial \zeta}\right)^2 + 2A^2 \\&+ M \left(A - \frac{\partial f(\zeta;s)}{\partial \zeta}\right) + (Gr \theta(\zeta;s) + Gc \phi(\zeta;s)) \cos \Omega,\end{aligned}\quad (18)$$

$$\begin{aligned}N_\theta[f(\zeta;s), \theta(\zeta;s), \phi(\zeta;s)] \\= \frac{1}{Pr} \left(1 + \frac{4}{3} R\right) \frac{\partial^2 \theta(\zeta;s)}{\partial \zeta^2} \\+ f(\zeta;s) \frac{\partial \theta(\zeta;s)}{\partial \zeta} - \theta(\zeta;s) \frac{\partial f(\zeta;s)}{\partial \zeta} \\+ Nb \frac{\partial \theta(\zeta;s)}{\partial \zeta} \frac{\partial \phi(\zeta;s)}{\partial \zeta} + Nt \left(\frac{\partial \theta(\zeta;s)}{\partial \zeta}\right)^2 \\+ Q \theta(\zeta;s),\end{aligned}\quad (19)$$

$$\begin{aligned}N_\phi[f(\zeta;s), \theta(\zeta;s), \phi(\zeta;s)] &= \frac{\partial^2 \phi(\zeta;s)}{\partial \zeta^2} \\&+ Sc \left(f(\zeta;s) \frac{\partial \phi(\zeta;s)}{\partial \zeta} - \phi(\zeta;s) \frac{\partial f(\zeta;s)}{\partial \zeta}\right) \\&+ \frac{Nt}{Nb} \frac{\partial^2 \theta(\zeta;s)}{\partial \zeta^2} - Sc \gamma \phi(\zeta;s),\end{aligned}\quad (20)$$

The value of p (embedding parameter) lies between 0 and 1 (including end points), s the embedding constraint, h_f, h_θ and h_ϕ are non-zero auxiliary constraints and N_f, N_θ and N_ϕ are operators of nonlinear terms.

In the following, the n th-order deformation equations are presented:

$$M_f(f_n(\zeta) - \chi_n f_{n-1}(\zeta)) = h_f R_n^f(\zeta), \quad (21)$$

$$M_\theta(\theta_n(\zeta) - \chi_n \theta_{n-1}(\zeta)) = h_\theta R_n^\theta(\zeta), \quad (22)$$

$$M_\phi(\phi_n(\zeta) - \chi_n \phi_{n-1}(\zeta)) = h_\phi R_n^\phi(\zeta), \quad (23)$$

with the following boundary conditions:

$$\begin{aligned}f_n(0) &= 0, \\f'_n(0) &= \delta_1 \left(1 + \frac{1}{\beta}\right) f''_n(0), \\f'_n(\infty) &\rightarrow 0, \\ \theta_n(0) &= \delta_2 \theta'_n(0), \quad \theta_n(\infty) \rightarrow 0, \\ \phi_n(0) &= \delta_3 \phi'_n(0), \quad \phi_n(\infty) \rightarrow 0,\end{aligned}\quad (24)$$

where,

$$\begin{aligned}R_n^f(\zeta) &= \left(1 + \frac{1}{\beta}\right) f'''_{n-1} + 2 \sum_{i=0}^{n-1} f_{n-1-i} f''_i \\&- \sum_{i=0}^{n-1} f'_{n-1-i} f'_i + (1 - \chi_n) (2A^2 + M) - M f'_{n-1} \\&+ (Gr \theta_{n-1} + Gc \phi_{n-1}) \cos \Omega\end{aligned}\quad (25)$$

$$\begin{aligned}R_n^\theta(\zeta) &= \frac{1}{Pr} \left(1 + \frac{4R}{3}\right) \theta''_{n-1} + \sum_{i=0}^{n-1} (f_{n-1-i} \theta'_i - \theta_{n-1-i} f'_i) \\&+ Nb \sum_{i=0}^{n-1} \theta'_{n-1-i} \phi'_i + Nt \sum_{i=0}^{n-1} \theta'_{n-1-i} \theta'_i + Ec \sum_{i=0}^{n-1} f_{n-1-i} f''_i,\end{aligned}\quad (26)$$

$$\begin{aligned}R_n^\phi(\zeta) &= \phi''_{n-1} \\&+ Sc \left(\sum_{i=0}^{n-1} f_{n-1-i} \phi'_i - \sum_{i=0}^{n-1} \phi_{n-1-i} f'_i - \gamma \phi_{n-1}\right) + \frac{Nt}{Nb} \theta''_{n-1},\end{aligned}\quad (27)$$

$$\chi_n = \begin{cases} 0, & n \leq 1, \\ 1, & n > 1. \end{cases}$$

If we let $f_n^*(\zeta)$, $\theta_n^*(\zeta)$ and $\phi_n^*(\zeta)$, the general solution of the n th order deformation equations is provided by the special solutions of:

$$\begin{aligned} f_n(\zeta) &= f_n^*(\zeta) + D_1 + D_2 e^\zeta + D_3 e^{-\zeta}, \\ \theta_n(\zeta) &= \theta_n^*(\zeta) + D_4 e^\zeta + D_5 e^{-\zeta}, \\ \phi_n(\zeta) &= \phi_n^*(\zeta) + D_6 e^\zeta + D_7 e^{-\zeta}, \end{aligned} \tag{28}$$

where, the integral constants $D_i(i=1$ to $7)$ are determined using the boundary conditions.
The aforementioned linear homogeneous equations can be easily solved using MATHEMATICA in the following order: $n=1,2, \dots$

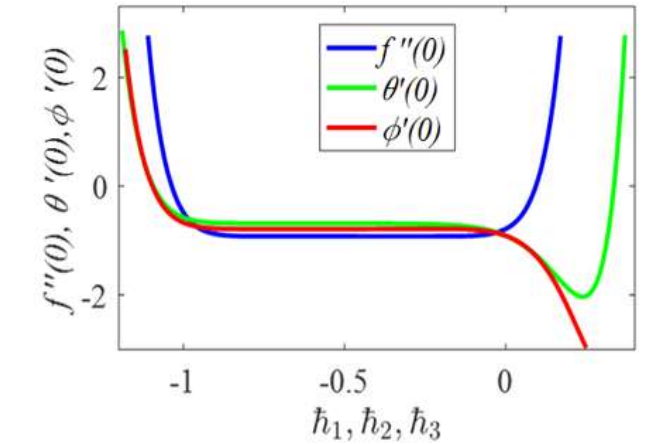


Figure 3. h -curves for $f''(0), \theta'(0)$ and $\phi'(0)$ at 15th order approximations

Table 1. Convergence behavior of HAM solutions at various approximation orders

Order	$-f''(0)$	$-\theta'(0)$	$-\phi''(0)$
5	0.921021	0.685804	0.784599
10	0.919537	0.682007	0.787443
15	0.919644	0.681943	0.787599
20	0.919632	0.681942	0.787595
25	0.919633	0.681942	0.787595
30	0.919633	0.681942	0.787595
35	0.919633	0.681942	0.787595
40	0.919633	0.681942	0.787595

To determine the appropriate values for the auxiliary parameters that are not zero, h -curves are portrayed in Figure 3. From this figure, the presumable interval of auxiliary parameter is $[-1.0, 0.0]$. The solutions are convergent for whole region of ζ when $h_f = h_\theta = h_\phi = -0.69$. Integration of the method is given in Table 1.

5. RESULTS AND DISCUSSIONS

Boundary conditions have been addressed by taking advantage of the modified equations that have been exposed to HAM. Graphs are plotted for different profiles for varying values of the controlling constraints. To determine the validity of our effort, a comparison with historical trends was conducted, and Table 2 clearly shows the enormous agreement we obtained. While most of the figures are generated by varying a specific parameter over a range of values, some remain fixed at a single value throughout the entire simulation, such as $\beta = 1.0, M=0.5, A=0.5, \Omega = 60^\circ, S=0.5, Gr=0.5, Gc=0.5, \delta_1 = \delta_2 = \delta_3 = 0.3, R=0.5, Pr=0.71, Q=0.5, Nb=0.5, Nt=0.5, Sc=0.6$, and $\gamma = 0.5$.

The way the momentum is affected by the Casson fluid parameter β , thermal & solutal contours were revealed in Figures 4 to 6. Amplification in β has been found to decline the fluid's viscosity. As a change in β causes the fluid to behave like shear-thickening, which diminishes the fluid's fluidity and the width of its momentum barrier layer. While the velocity contour displays the opposite tendency, the thermal, solutal contours grow as the Casson fluid parameter increases.

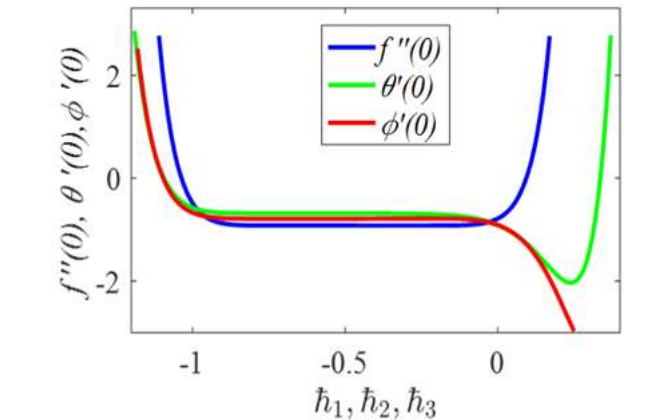


Figure 4. Figuration of $f'(\zeta)$ for β

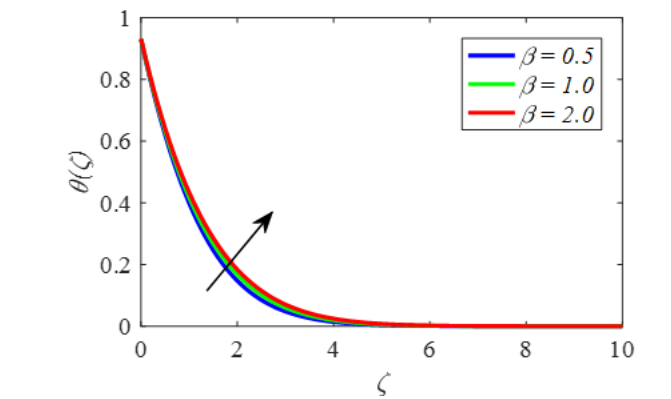


Figure 5. Figuration of $\theta(\zeta)$ for β

Table 2. Comparison of $-\theta'(0)$ for various values of M, Pr and R in the absence of remaining constraints

M	R	Pr	Bidin and Nazar [42]	Ishak [43]	Rajendar and Anand Babu [44]	HAM
0.0	0.0	1.0	0.9547	0.9547	0.9548	0.954783
0.0	0.0	3.0	1.8691	1.8691	1.8692	1.869067
0.0	1.0	1.0	0.5315	0.5315	0.5311	0.531503
1.0	0.0	1.0	0.8611	--	0.8611	0.861427

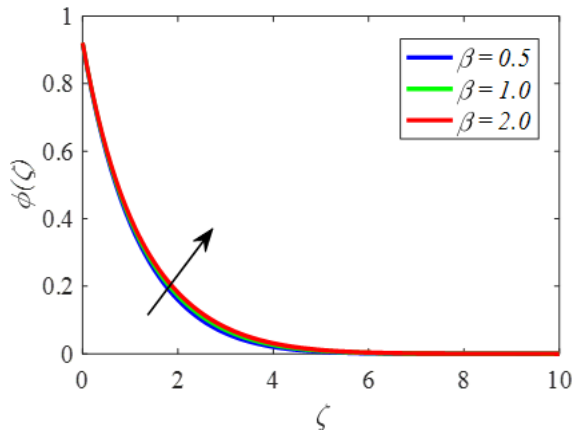


Figure 6. Figuration of $\phi(\zeta)$ for β

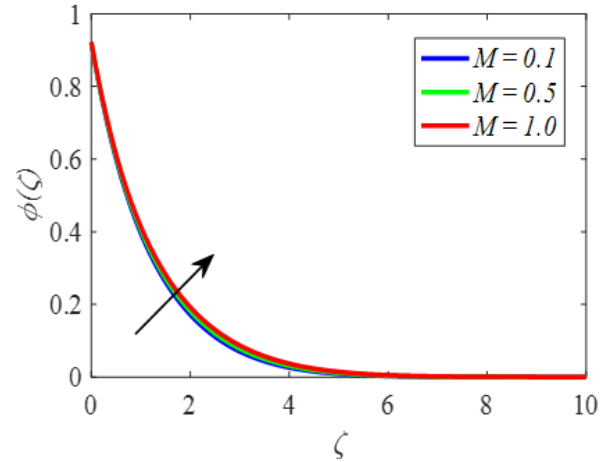


Figure 9. Figuration of $\phi(\zeta)$ for M

Figures 7 to 9 validate that the magnetic parameter M affects the profiles. Although the trend for concentration and temperature is the reverse, $f'(\zeta)$ falls as M 's magnitude upsurges. The rate of transfer actually declines as M increases as a result of which it upsurges the Lorentz force that limits the flow of fluids. The Lorentz force was visible when the flow field was going through a magnetic field. This force is powerful enough to drag the fluid along and slow its movement. Consequently, the fluid flow momentum decreases as the velocity layer thickness increases.

Figure 10 exemplifies that the momentum ratio significator A affects the momentum of the profiles. The fluid's momentum gains as the momentum ratio significator the magnitude upsurges. Figures 11 and 12 display the momentum ratio significator. A affects the development of non-dimensional thermal and solutal contours. As A surge, the thermal and solutal of the fluid asymptotically decline, forming thin temperature and concentration boundary layers. A greater momentum ratio signifies more. The momentum of the free stream is increased by heat transfer from the wall. The concentration of the fluid upsurges in tandem with the free stream velocity as momentum ratio significator A upsurges.

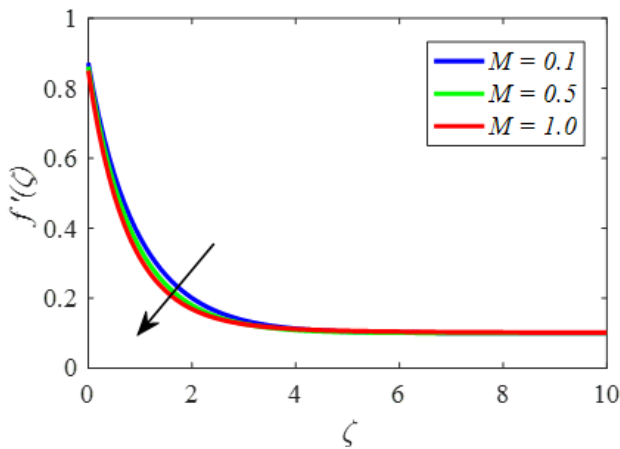


Figure 7. Figuration of $f'(\zeta)$ for M

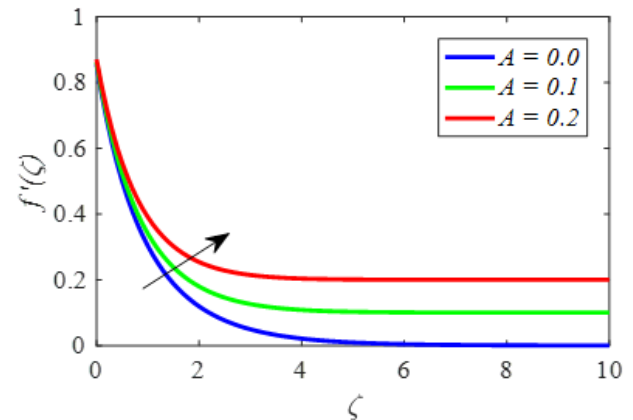


Figure 10. Figuration of $f'(\zeta)$ for A

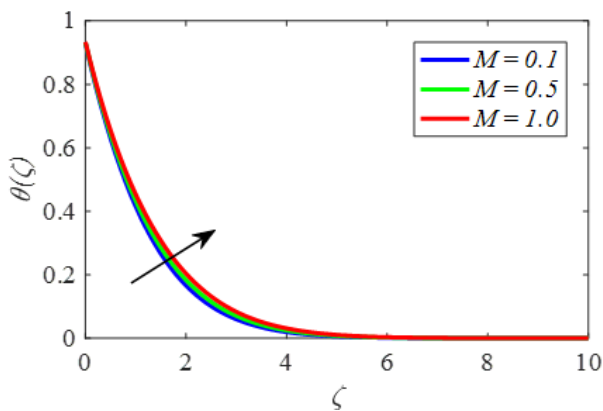


Figure 8. Figuration of $\theta(\zeta)$ for M

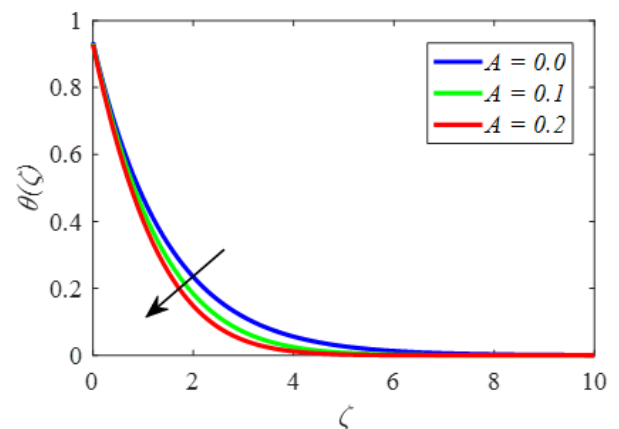


Figure 11. Figuration of $\theta(\zeta)$ for A

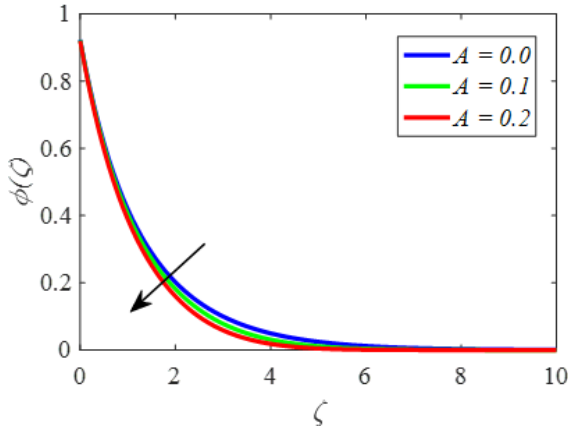


Figure 12. Figuration of $\phi(\zeta)$ for A

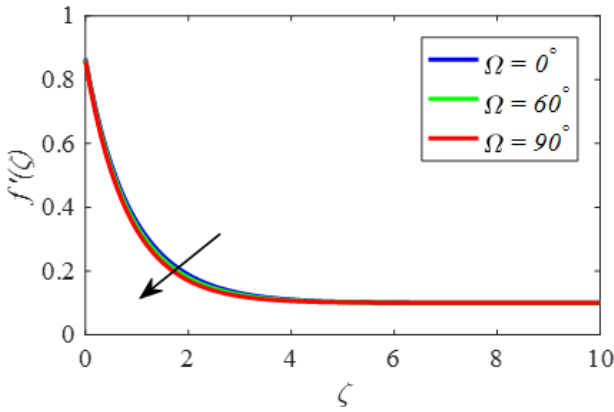


Figure 13. Figuration of $f'(\zeta)$ for Ω

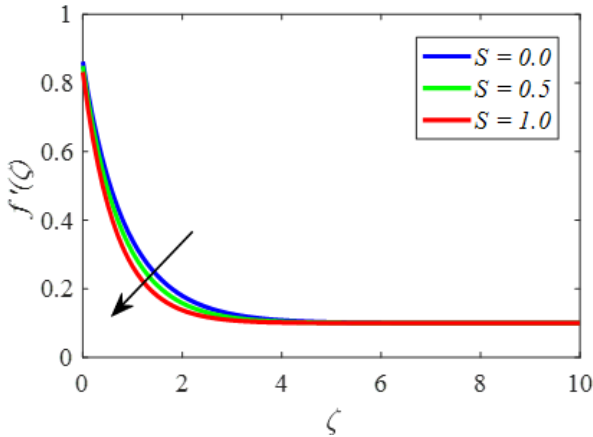


Figure 14. Figuration of $f'(\zeta)$ for S

The impact of an inclined angle on the momentum contour is illustrated in Figure 13. As the increases, the momentum contour decreases. This is explained by the fact that the buoyant force caused by thermal diffusion is reduced by a factor of $\cos \Omega$. As higher values suction (S) effectively reduce the momentum contour both in fluid and gaseous forms, as shown in Figure 14. The features of the local Grashof number are Gr on the momentum contours are depicted in Figure 15. In this case, the fluid flow velocity will increase quickly as Gr values rise.

Figure 16 demonstrates that the velocity contours improve when the adjusted Grashof parameter G_c values upsurge. Figure 17 depicts the restriction on velocity slip δ_1 upsurges,

the fluid speed falls and the slip speed upsurges. This could be because the velocity of the stream and the stretched sheet are different in the case of a slip scenario. An upsurge in the velocity slip limitation δ_1 causes the fluid velocity to drop as the slip velocity increases. This phenomenon occurs when, in slip conditions, the velocity of the fluid stream close to the stretching sheet differs from that of the document for extending. As the thermal slip limitation δ_2 rises, Figure 18 demonstrates that the temperature declines. Although there is very little heat and the physical width of the temperature boundary layer decreases as the thermal slip constraint value increases during the transfer from the sheet to the temperature boundary layer.

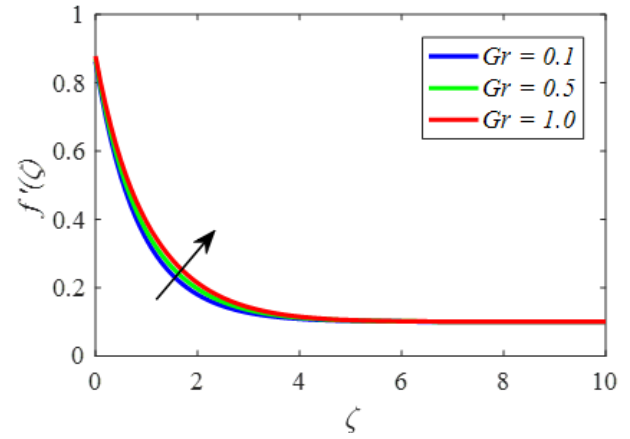


Figure 15. Figuration of $f'(\zeta)$ for Gr

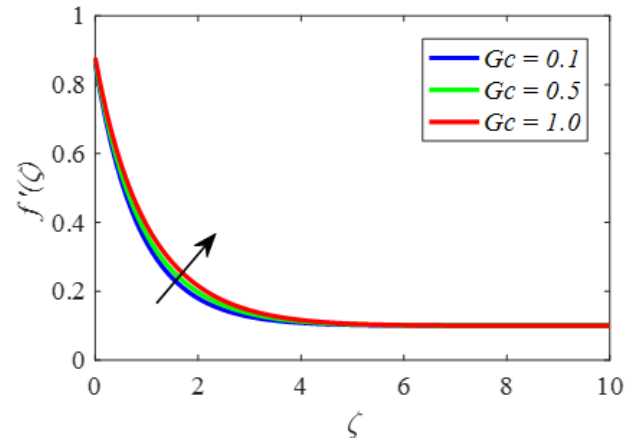


Figure 16. Figuration of $f'(\zeta)$ for G_c

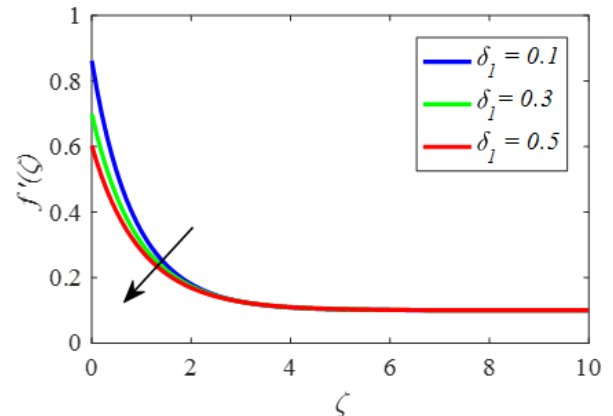


Figure 17. Figuration of $f'(\zeta)$ for δ_1

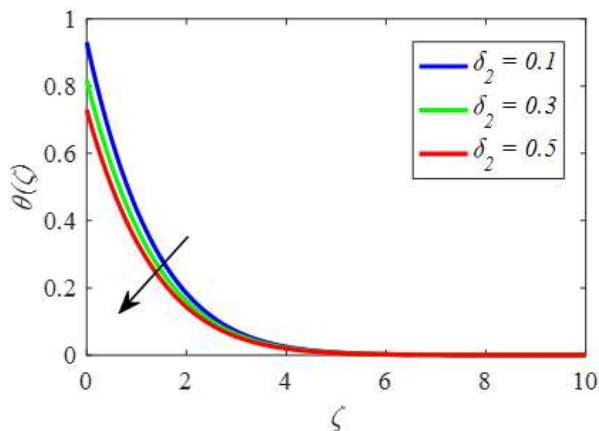


Figure 18. Figation of $\theta(\zeta)$ for δ_2

Figure 19 shows the connection between thermal radiation and temperature limitation R . Higher values of R indicate a greater infusion of heat energy that radiates into the system, raising the temperature. Figure 20 displays the temperature contours change for different Prandtl values. The Prandtl number is found to be upsurges, the boundary layer's thermal declines. The extraordinary effect of Q on $\theta(\zeta)$ is revealed in Figure 21. An increase in the values improves θ in the case of air. The thermal contour initially declines before rising away from the wall.

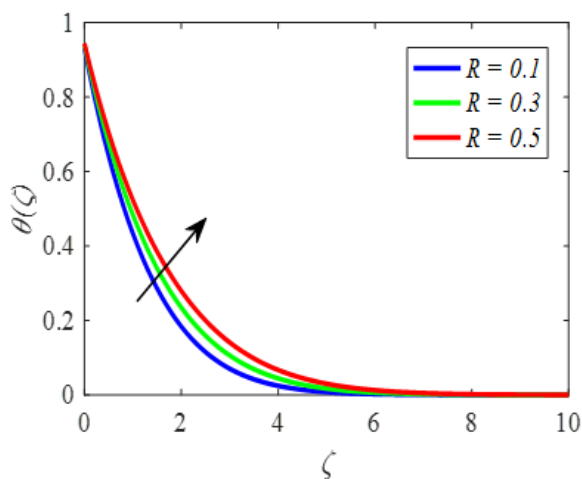


Figure 19. Figation of $\theta(\zeta)$ for R

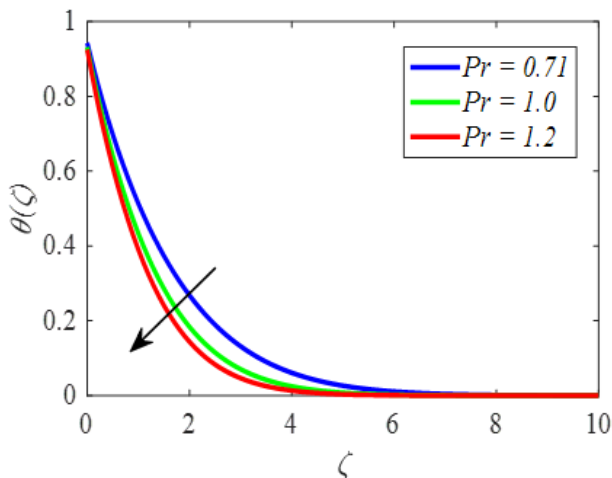


Figure 20. Figation of $\theta(\zeta)$ for Pr

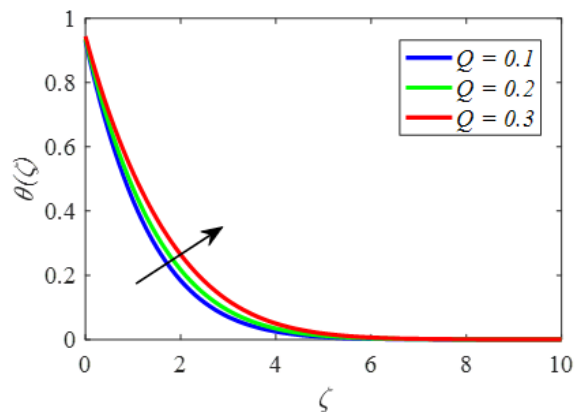


Figure 21. Figation of $\theta(\zeta)$ for Q

Figure 22 illustrates the significance of the Brownian movement significator in a clear and concise manner. Nb may have an effect on $\theta(\zeta)$. In general, Brownian mobility helps to regulate the temperature of the fluid in the boundary layer by preventing materials from accumulating on the surface that is located at a distance from the fluid. The temperature rises when there is a greater concentration of Nb in the fluid (one that is less than 1). Most of the time, Brownian motion is responsible for preventing molecules from depositing away from the surface of the liquid and warming the liquid that is contained within the boundary layer. At some distance from the extension surface, rapid flow is brought about by the thermophoretic force that is produced by the temperature gradient that is the result of the extension. As Nb increases, a greater quantity of fluid is heated away from the surface, which results in an increase in the thermal properties of the boundary layer. However, concentration profiles exhibit the reverse pattern, as illustrated in Figure 23.

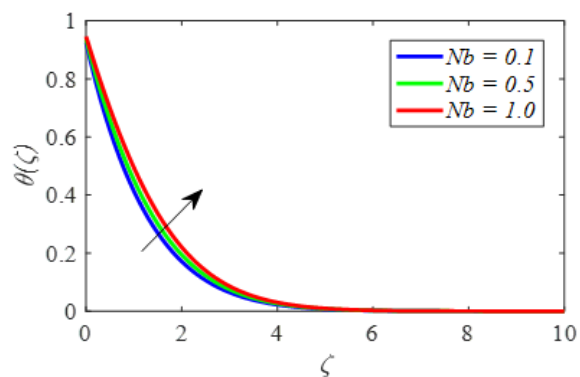


Figure 22. Figation of $\theta(\zeta)$ for Nb

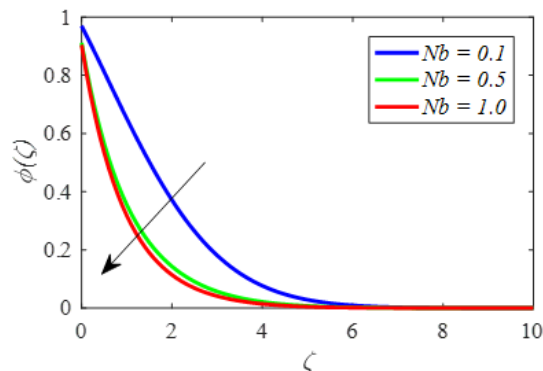


Figure 23. Figation of $\phi(\zeta)$ for Nb

The stretched sheet creates a rapid flow that carries nanoparticles, widening the boundary layer for the mass volume fraction. These phenomena are demonstrated in Figures 24 and 25. It has been reported that Nt directly correlates with both the thermal and the solutal of nanoparticles.

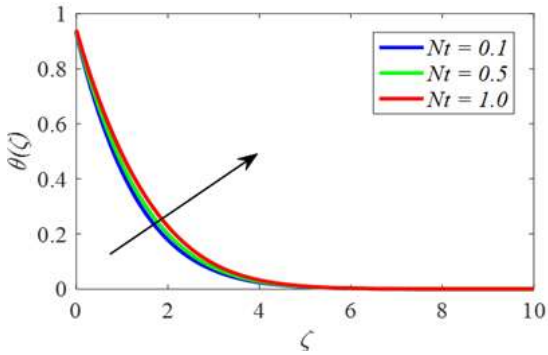


Figure 24. Figuration of $\theta(\zeta)$ for Nt

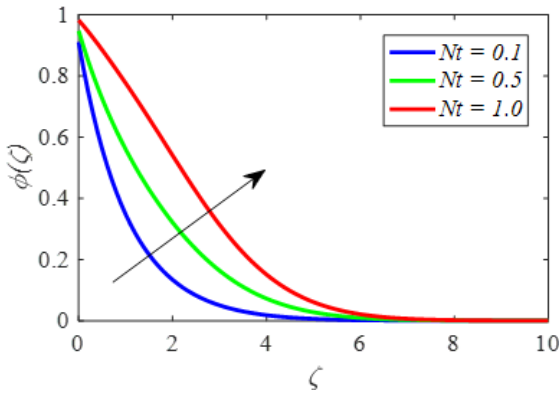


Figure 25. Figuration of $\phi(\zeta)$ for Nt

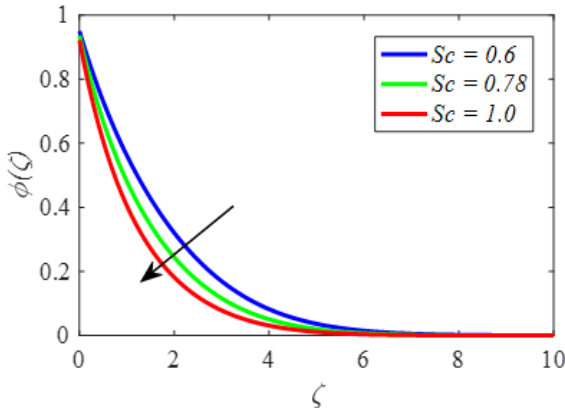


Figure 26. Figuration of $\phi(\zeta)$ for Sc

Figure 26 portrays the Schmidt number (Sc) affects the $\phi(\zeta)$ concentration contour. Additionally, it has been noted that when the value grows, the concentration contour falls. A lower mass diffusivity relative to velocity diffusivity is indicated by a higher Schmidt number, which implies a decrease in scalar diffusivity, less diffusion, and slower solutal changes in the fluid medium. The ratio of mass diffusivity to momentum diffusivity is known as Sc in physics. The effect of a chemical reaction signicator γ on $\phi(\zeta)$ is portrayed in Figure 27. It is well known that when the chemical reaction

significance increases, the solutal falls. Figure 28 exemplifies the nanoparticle fraction slip limitation δ_3 has a similar effect on the mass fraction field as it does on the temperature field. This resemblance results from slip's fundamental obstruction to liquid motion, which ultimately lowers net atomic advancement. Consequently, reduced molecular development leads to a decline in the mass fraction field.

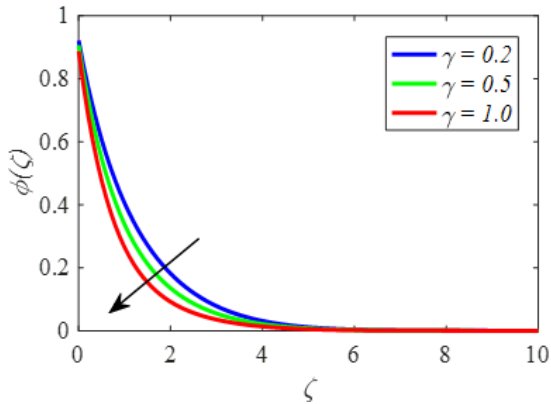


Figure 27. Figuration of $\phi(\zeta)$ for γ

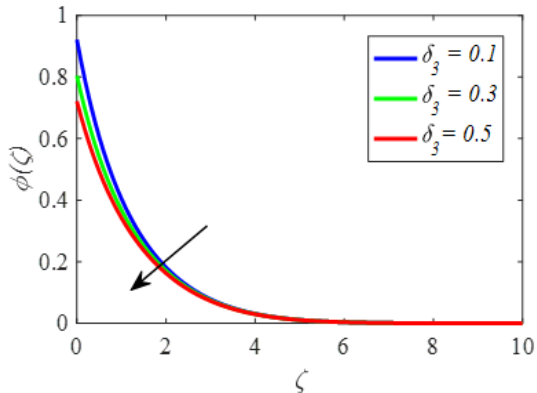


Figure 28. Figuration of $\phi(\zeta)$ for δ_3

Figure 29 exhibits the skin-friction factor on variation β and M . It's observed that as β and M heightened the skin-friction factor declines. Figure 30 demonstrated that the Nusselt number on variations of β and M . It is observed that as β and M increased the Nusselt number declines. Figure 31 depicted that the local Sherwood number on variations of β and M . It is noticed that as β and M . increased the local Sherwood number declines.

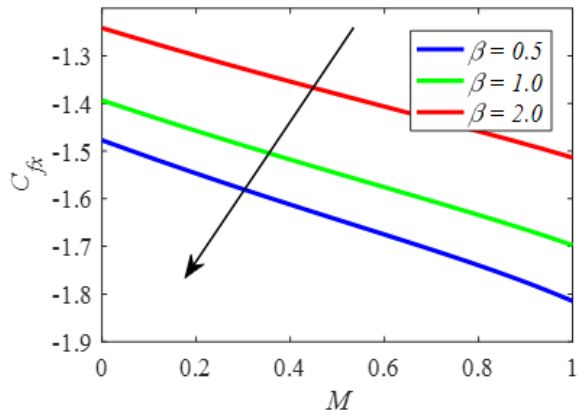


Figure 29. Figuration of C_{fx} for β and M

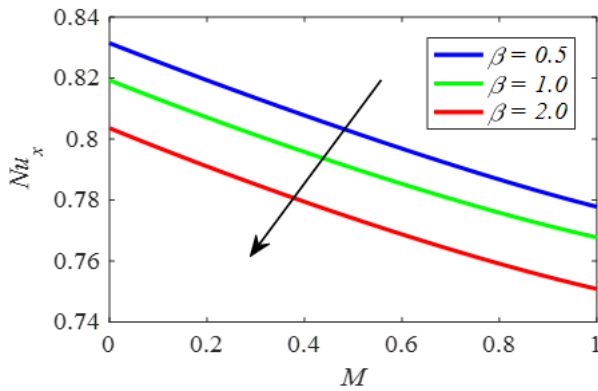


Figure 30. Figuration of Nu_x for β and M

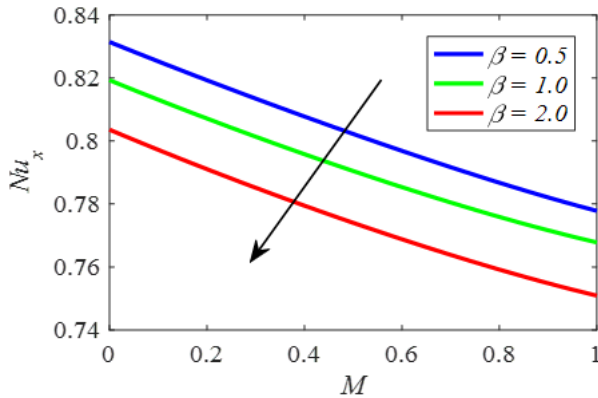


Figure 31. Figuration of Sh_x for β and M

6. CONCLUSIONS

Based on the results of numerical analysis that were carried out using a HAM technique, the following conclusions were derived regarding the MHD features of a Casson nanofluid that was flowing over an inclined stretching sheet that was stretched linearly:

- When the momentum of the nanofluid declines, the Casson constraint, the magnetic constraint, and the momentum slip factor all have an impact on the degree to which this can occur. A rise in the thermal characteristics of the nanofluid is brought about by the combination of three constraints: the heat source constraint, the Brownian motion constraint, and the temperature radiation constraint.
- As the Casson constraint and the thermophoresis constraint both increase, the solution boundary layer also increases, but it decreases as the Brownian motion component decreases.
- The momentum slip constraint and increases in the heat and mass transfer rates are directly related to one another. There is a correlation between the two. However, as the thermal leap constraint values grow, both the rate of heat transfer and the rate of mass transfer decrease. This is the case.
- In the event that the magnetic constraint is increased, it has been seen that the Sherwood and Nusselt numbers subsequently fall. In the event that momentum slip takes place, both the Sherwood number and the Nusselt number will decrease.

It is possible that in our subsequent research attempts, we will broaden the scope of the work that we are currently doing in order to encompass the non-Newtonian flow across a nonlinear stretching sheet and to consider hybrid nanofluids.

REFERENCES

- [1] Casson, N. (1959). Flow equation for pigment-oil suspensions of the printing ink-type. In *Rheology of Disperse Systems*, Pergamon Press, Oxford, 84-104.
- [2] Reddy, P.B.A. (2016). Magnetohydrodynamic flow of a Casson fluid over an exponentially inclined permeable stretching surface with thermal radiation and chemical reaction. *Ain Shams Engineering Journal*, 7(2): 593-602. <https://doi.org/10.1016/j.asej.2015.12.010>
- [3] Walawender, W.P., Chen, T.Y., Cala, D.F. (1975). An approximate Casson fluid model for tube flow of blood. *Biorheology*, 12(2): 111-119. <https://doi.org/10.3233/BIR-1975-12202>
- [4] Dash, R.K., Mehta, K.N., Jayaraman, G. (1996). Casson fluid flow in a pipe filled with a homogeneous porous medium. *International Journal of Engineering Science*, 34(10): 1145-1156. [https://doi.org/10.1016/0020-7225\(96\)00012-2](https://doi.org/10.1016/0020-7225(96)00012-2)
- [5] Mukhopadhyay, S., De, P.R., Bhattacharyya, K., Layek, G.C. (2013). Casson fluid flow over an unsteady stretching surface. *Ain Shams Engineering Journal*, 4(4): 933-938. <https://doi.org/10.1016/j.asej.2013.04.004>
- [6] Pramanik, S. (2014). Casson fluid flow and heat transfer past an exponentially porous stretching surface in presence of thermal radiation. *Ain Shams Engineering Journal*, 5(1): 205-212. <https://doi.org/10.1016/j.asej.2013.05.003>
- [7] Rao, P.S., Prakash, O., Mishra, S.R., Sharma, R.P. (2020). Similarity solution of three-dimensional MHD radiative Casson nanofluid motion over a stretching surface with chemical and diffusion-thermo effects. *Heat Transfer*, 49(4): 1842-1862. <https://doi.org/10.1002/htj.21696>
- [8] Choi, U.S. (1995). Enhancing thermal conductivity of fluids with nanoparticles, In: D.A. Siginer and H.P. Wang Eds., *Developments and Applications of Non-Newtonian flows*, ASME, New York, 99-105.
- [9] Reddy, R.C.S., Ramasekhar, G. (2023). Enhanced heat transfer analysis on MHD hybrid nanofluid flow over a porous stretching surface. An application to aerospace features. *East European Journal of Physics*, 4: 286-293. <https://doi.org/10.26565/2312-4334-2023-4-36>
- [10] Dzulkifli, N.F., Bachok, N., Yacob, N.A.M., Arifin, N.M., Rosali, H. (2017). Unsteady boundary layer rotating flow and heat transfer in a copper-water nanofluid over a stretching sheet. *Malaysian Journal of Mathematical Sciences*, 1830(1): 020050. <https://doi.org/10.1063/1.4980913>
- [11] Lund, L.A., Omar, Z., Raza, J., Khan, I., Sherif, E.S.M. (2020). Effects of Stefan blowing and slip conditions on unsteady MHD Casson nanofluid flow over an unsteady shrinking sheet: Dual solutions. *Symmetry*, 12(3): 487. <https://doi.org/10.3390/sym12030487>
- [12] Shah, J., Ali, F., Khan, N., Ahmad, Z., Murtaza, S., Khan, I., Mahmoud, O. (2022). MHD flow of time-fractional Casson nanofluid using generalized Fourier and Fick's laws over an inclined channel with applications of gold nanoparticles. *Scientific Reports*, 12: 17364.

- <https://doi.org/10.1038/s41598-022-21006-9>
- [13] Rehman, A., Khan, D., Mahariq, I., Elkotb, M.A., Elnaqeeb, T. (2024). Viscous dissipation effects on time-dependent MHD Casson nanofluid over stretching surface: A hybrid nanofluid study. *Journal of Molecular Liquids*, 408: 125370. <https://doi.org/10.1016/j.molliq.2024.125370>
- [14] Panigrahi, L., Panda, J., Swain, K., Dash, G.C. (2020). Heat and mass transfer of MHD Casson nanofluid flow through a porous medium past a stretching sheet with Newtonian heating and chemical reaction. *Karbala International Journal of Modern Science*, 6(3): 11. <https://doi.org/10.33640/2405-609X.1740>
- [15] Irshad, S., Jahan, S., Machado, J.M. (2025). MHD Casson flow across a stretched surface in a porous material: A numerical study. *Multiscale and Multidisciplinary Modeling, Experiments and Design*, 8: 36. <https://doi.org/10.1007/s41939-024-00628-8>
- [16] Chaudhary, S., Kanika, K.M. (2020). Heat generation/absorption and radiation effects on hydromagnetic stagnation point flow of nanofluids toward a heated porous stretching/shrinking sheet with suction/injection. *Journal of Porous Media*, 23(1): 27-49. <https://doi.org/10.1615/JPorMedia.2019026922>
- [17] Reddy, Y.D., Mebarek-Oudina, F., Goud, B.S., Ismail, A.I. (2022). Radiation, velocity and thermal slips effect toward MHD boundary layer flow through heat and mass transport of Williamson nanofluid with porous medium. *Arabian Journal for Science and Engineering*, 47(12): 16355-16369. <https://doi.org/10.1007/s13369-022-06825-2>
- [18] Pal, D., Mandal, G. (2014). Influence of thermal radiation on mixed convection heat and mass transfer stagnation-point flow in nanofluids over stretching/shrinking sheet in a porous medium with chemical reaction. *Nuclear Engineering and Design*, 273: 644-652. <https://doi.org/10.1016/j.nucengdes.2014.01.032>
- [19] Megahed, A.M., Abbas, W. (2022). Non-Newtonian cross fluid flow through a porous medium with regard to the effect of chemical reaction and thermal stratification phenomenon. *Case Studies in Thermal Engineering*, 29: 101715. <https://doi.org/10.1016/j.csite.2021.101715>
- [20] Barik, A.K., Mishra, S.K., Mishra, S.R., Pattnaik, P.K. (2020). Multiple slip effects on MHD nanofluid flow over an inclined, radiative, and chemically reacting stretching sheet by means of FDM. *Heat Transfer—Asian Research*, 49(1): 477-501. <https://doi.org/10.1002/htj.21622>
- [21] Sadaf, H., Akbar, M.U., Nadeem, S. (2018). Induced magnetic field analysis for the peristaltic transport of non-Newtonian nanofluid in an annulus. *Mathematics and Computers in Simulation*, 148: 16-36. <https://doi.org/10.1016/j.matcom.2017.12.009>
- [22] Ramana, R.M., Raju, K.V., Kumar, J.G. (2022). Multiple slips and heat source effects on MHD stagnation point flow of Casson fluid over a stretching sheet in the presence of chemical reaction. *Materials Today: Proceedings*, 49: 2306-2315. <https://doi.org/10.1016/j.matpr.2021.09.348>
- [23] Nandi, S., Kumbhakar, B., Sarkar, S. (2022). MHD stagnation point flow of $\text{Fe}_3\text{O}_4/\text{Cu}/\text{Ag}-\text{CH}_3\text{OH}$ nanofluid along a convectively heated stretching sheet with partial slip and activation energy: Numerical and statistical approach. *International Communications in Heat and Mass Transfer*, 130: 105791. <https://doi.org/10.1016/j.icheatmasstransfer.2021.105791>
- [24] Thabet, E.N., Khan, Z., Abd-Alla, A.M., Bayones, F.S. (2023). Thermal enhancement, thermophoretic diffusion, and Brownian motion impacts on MHD micropolar nanofluid over an inclined surface: numerical simulation. *Numerical Heat Transfer, Part A: Applications*, 86(4): 871-890. <https://doi.org/10.1080/10407782.2023.2276319>
- [25] Shahzad, A., Imran, M., Tahir, M., Khan, S.A., Akgül, A., Abdullaev, S., Park, C., Zahran, H.Y., Yahia, I.S. (2023). Brownian motion and thermophoretic diffusion impact on Darcy–Forchheimer flow of bioconvective micropolar nanofluid between double disks with Cattaneo–Christov heat flux. *Alexandria Engineering Journal*, 62: 1-15. <https://doi.org/10.1016/j.aej.2022.07.023>
- [26] Hazarika, S., Ahmed, S. (2022). Brownian motion and thermophoresis behavior on micro-polar nano-fluid—A numerical outlook. *Mathematics and Computers in Simulation*, 192: 452-463. <https://doi.org/10.1016/j.matcom.2021.09.002>
- [27] Irfan, M. (2021). Study of Brownian motion and thermophoretic diffusion on nonlinear mixed convection flow of Carreau nanofluid subject to variable properties. *Surfaces and Interfaces*, 23: 100926. <https://doi.org/10.1016/j.surfin.2021.100926>
- [28] Shah, N.A., Tosin, O., Shah, R., Salah, B., Chung, J.D. (2021). Brownian motion and thermophoretic diffusion effects on the dynamics of MHD upper convected Maxwell nanofluid flow past a vertical surface. *Physica Scripta*, 96(12): 125722. <https://doi.org/10.1088/1402-4896/ac36ea>
- [29] Medebber, M.A., Zeng, S., Retiel, N. (2025). Magnetohydrodynamic laminar natural convection in a two-dimensional trapezoidal porous cavity filled with hybrid nanofluid ($\text{Al}_2\text{O}_3\text{-Cu/water}$) flow: Entropy generation. *International Journal of Heat and Technology*, 43(2): 381-390. <https://doi.org/10.18280/ijht.430201>
- [30] Anjum, A., Kumar, D.S., Gaffar, S.A., Peerusab, S. (2025). Heat and mass transfer in magneto-Dissipative Boussinesq Nanofluid flow along a semi-infinite plate in a non-Darcy porous medium. *International Journal of Heat and Technology*, 43(2): 583-602. <https://doi.org/10.18280/ijht.430220>
- [31] Nadhim, A.A., Alderoubi, N., Ali Al-Tammermi, O.H., Mustafa, M.A.S., Majdi, H.S. (2024). Numerical study of heat transfer in helical cone coil heat exchanger using MWCNT-water nanofluid. *International Journal of Heat and Technology*, 42(5): 1567-1577. <https://doi.org/10.18280/ijht.420510>
- [32] Ramadevu, S., Prathi, V., Thota, N.R., Shaik, M.I., Kanithi, J. (2025). Flow and heat transfer analysis of jeffrey nanofluid over a Nonlinear stretching sheet with porous medium and slip effects: HAM-based solutions. *Journal of Advanced Research in Numerical Heat Transfer*, 30(1): 120-146. <https://doi.org/10.37934/arnht.30.1.120146>
- [33] Ramadevu, S., Vijaya Kumar, P., Ibrahim, S.M., Jyothsna, K. (2025). Investigation of heat and mass transfer in magnetohydrodynamic Williamson nanofluid flow over a nonlinear stretching surface with viscous

- dissipation and radiation effects: A numerical approach. *Radiation Effects and Defects in Solids*, 1-22. <https://doi.org/10.1080/10420150.2025.2467348>
- [34] Jawad, M. (2023). A computational study on magnetohydrodynamics stagnation point flow of micropolar fluids with buoyancy and thermal radiation due to a vertical stretching surface. *Journal of Nanofluids*, 12(3): 759-766. <https://doi.org/10.1166/jon.2023.1983>
- [35] Pera, L., Gebhart, B. (1973). Natural convection boundary layer flow over horizontal and slightly inclined surfaces. *International Journal of Heat and Mass Transfer*, 16(6): 1131-1146. [https://doi.org/10.1016/0017-9310\(73\)90126-9](https://doi.org/10.1016/0017-9310(73)90126-9)
- [36] Raju, R.S. (2018). Unsteady MHD boundary layer flow of Casson fluid over an inclined surface embedded in a porous medium with thermal radiation and chemical reaction. *Journal of Nanofluids*, 7(4): 694-703. <https://doi.org/10.1166/jon.2018.1500>
- [37] Rafique, K., Anwar, M.I., Misiran, M., Khan, I., Alharbi, S.O., Thounthong, P., Nisar, K.S. (2019). Numerical solution of Casson nanofluid flow over a non-linear inclined surface with Soret and Dufour effects by Keller-box method. *Frontiers in Physics*, 7: 139. <https://doi.org/10.3389/fphy.2019.00139>
- [38] Tawade, J.V., Guled, C.N., Noeiaghdam, S., Fernandez-Gamiz, U., Govindan, V., Balamuralitharan, S. (2022). Effects of thermophoresis and Brownian motion for thermal and chemically reacting Casson nanofluid flow over a linearly stretching sheet. *Results in Engineering*, 15: 100448. <https://doi.org/10.1016/j.rineng.2022.100448>
- [39] Pal, D., Chatterjee, D., Vajravelu, K. (2020). Influence of magneto-thermo radiation on heat transfer of a thin nanofluid film with non-uniform heat source/sink. *Propulsion and Power Research*, 9(2): 169-180. <https://doi.org/10.1016/j.jprr.2020.03.003>
- [40] Abbas, W., Megahed, A.M. (2021). Numerical solution for chemical reaction and viscous dissipation phenomena on non-Newtonian MHD fluid flow and heat mass transfer due to a nonuniform stretching sheet with thermal radiation. *International Journal of Modern Physics C*, 32(9): 2150124. <https://doi.org/10.1142/S0129183121501242>
- [41] Rao, M.E. (2018). The effects of thermal radiation and chemical reaction on MHD flow of a Casson fluid over an exponentially inclined stretching surface. *Journal of Physics: Conference Series*, 1000: 012158. <https://doi.org/10.1088/1742-6596/1000/1/012158>
- [42] Bidin, B., Nazar, R. (2009). Numerical solution of the boundary layer flow over an exponentially stretching sheet with thermal radiation. *European Journal of Scientific Research*, 33(4): 710-717.
- [43] Ishak, A. (2011). MHD boundary layer flow due to an exponentially stretching sheet with radiation effect. *Sains Malaysiana*, 40(4): 391-395.
- [44] Rajendar, P., Anand, B.L. (2018). MHD stagnation point flow of Williamson nanofluid over an exponentially inclined stretching surface with thermal radiation and viscous dissipation, *Journal of Nanofluids*, 7(4): 683-693. <https://doi.org/10.1166/jon.2018.1493>
- b free stream rate
- $(c)_f$ specific heat at non-varying pressure, $J.kg^{-1}.K^{-1}$
- u, v resolution of velocity vector along x,y directions, $m.s^{-1}$
- U_w stretching velocity, $m.s^{-1}$
- U_∞ free stream velocity, $m.s^{-1}$
- B_0 strength of magnetic field
- D_B coefficient of Brownian
- D_T coefficient of thermophoresis
- V_w wall injection/suction velocity
- π product of component deformation
- g gravitational acceleration $m.s^{-2}$
- R thermal radiation constraint
- C the fluid concentration, $kg.m^{-3}$
- C_w Solutal level of fluid at surface, $kg.m^{-3}$
- C_∞ concentration of the ambient, $kg.m^{-3}$
- k^* absorption coefficient
- κ heat conductance of fluid, $W.m^{-1}.K^{-1}$
- \hbar_f, \hbar_θ and \hbar_ϕ non-zero auxiliary parameters
- χ_n characteristic function
- $D_i (i = 1 \text{ to } 7)$ arbitrary constants
- N_f, N_θ and N_ϕ non-linear operators
- L_f, L_θ and L_ϕ linear operators
- M magnetic field constraint
- Nt thermophoresis constraint
- Nb Brownian motion constraint
- Pr Prandtl number
- Gr local Grashof number as a result of temperature changes
- Gc due to the level of concentration, the local Grashof number
- V_0 initial strength of suction
- C_{fx} coefficient of skin friction
- Sh_x local Nusselt number
- f local Sherwood number
- f' stream function with no dimension
- Sc dimensionless velocity
- Q Schmidt number
- Le heat source constraint
- T Lewis constraint
- T_w fluid's thermal K
- T_∞ convective liquid temperature
- q_w ambient fluid temperature, K
- q_m surface heat flow, $W.m^{-2}$
- τ_w surface mass movement
- τ_w shearing stress of the Surface, $N.m^{-2}$

Greek symbols

- μ_B plastic dynamic viscosity, $kg. M^{-1}.s^{-1}$
- γ chemical reaction parameter
- ζ similarity variable
- α diffusivity of the fluid at varying

NOMENCLATURE

- a constant extending rate

β_c	temperature	$\tau = \frac{(\rho c)_p}{(\rho c)_f}$	fraction of heat capability of Nanofluid to the base fluid
β_T	mass expansion coefficient in volume	σ_f	electrical conductivity, S.m ⁻¹
β	coefficient of mass expansion in volume units, K ⁻¹	ψ	stream function, m ² .s ⁻¹
σ^*	Casson constraint, K ⁻¹	ρ_p	nanoparticles mass density, kg.m ⁻³
ν	Stefan -Boltzmann constant	Subscripts	
ϕ	kinematic viscosity, m ² .s ⁻¹		
θ	dimensionless soluta		
$(\rho c)_f$	dimensionless Thermal		
Ω	fluid heat capacity		
	sheet angle with inclination	f	fluid (pure water)
		w	wall membrane
		∞	free stream